Copper-mediated metal-organic framework as efficient photocatalyst for the partial oxidation of aromatic alcohols under visible-light irradiation: Synergism of plasmonic effect and schottky junction

Liang Xiao[a], Qi Zhang[a], Peng Chen[a], Lang Chen[a,*], Feng Ding[a], Jie Tang[a], You-Ji Li[b], Chak-Tong Au[c], Shuang-Feng Yin[a,*]

[a] State Key Laboratory of Chemo/Biosensing and Chemometrics, Provincial Hunan Key Laboratory for Cost-effective Utilization of Fossil Fuel Aimed at Reducing Carbon-dioxide Emissions, College of Chemistry and Chemical Engineering, Hunan University, Changsha 410082, Hunan, China
[b] Key Laboratory of Mineral Cleaner Production and Exploit of Green Functional Materials in Hunan Province, Jishou University, Jishou 416000, Hunan, China
[c] College of Chemistry and Chemical Engineering, Hunan Institute of Engineering, Xiangtan 411104, Hunan, China

ABSTRACT

Metal-organic framework (MOF) is one of the most promising porous materials in photocatalysis. In this study, copper was deposited on as well as encapsulated in a semiconductor-like MOF (UiO-66) to fabricate the Cu/Cu@UiO-66 catalyst via an advanced double-solvent approach followed by one-step reduction. Even with ultralow amount of copper, Cu/Cu@UiO-66 shows significantly enhanced photocatalytic activity as well as stability for partial oxidation of aromatic alcohols under visible light irradiation. The result is attributed to the integration of plasmonic effect (Cu nanoparticles on UiO-66) and Schottky junction (Cu quantum dots encapsulated in UiO-66) which can be considered as a promising noble-metal-free way for the enhancement of visible-light-driven photocatalytic activity of MOFs.

1. Introduction

With high lowest unoccupied molecular orbital (LUMO) and low highest occupied molecular orbital (HOMO), most semiconductor-like metal-organic framework (MOF) permit UV light absorption and exhibit wide band gaps critical for high redox ability [1,2]. To broaden MOF application in photocatalysis, metal nanoparticles (NPs) with surface plasmon resonance (SPR) were loaded onto MOF of wide band gap to extend light absorption from UV to visible light region while maintaining their redox ability [3–8]. In addition, the encapsulation of metal NPs to form Schottky junctions has been reported as an effective way to enhance the transfer of photo-excited electrons and suppress re-combination of photo-induced electrons and holes [9–13]. It is envisaged that a combination of plasmonic effect and Schottky junctions would result in enhanced visible light photocatalytic activity of MOF.

Although progresses were made in this very field, the metals employed for the fabrication of composites were noble ones such as Pt, Ag and Au, and commonly two or more kinds of noble metals were used. Furthermore, to create a synergy between plasmonic effect and Schottky junction, the synthesis requires gradual introduction of external and internal components into the MOF. Unlike precious metals, copper is economical to use. Despite copper displays SPR under visible light irradiation, the use of this eco-friendly metal for the modification of MOF has rarely been investigated [14–16]. Moreover, copper provides active sites for the selective oxidation of alcohol to aldehyde [17–19].

With the above points in mind, we proceeded to investigate the integration of plasmonic Cu and Cu-MOF Schottky junction for the partial oxidation of aromatic alcohols under visible-light irradiation. We chose UiO-66 as a MOF representative and a UV-responsive photocatalyst because it is known to behave like a semiconductor of wide band gap [20–23]. As shown in Scheme 1, Cu quantum dots (QDs) could be encapsulated in UiO-66 by traditional double-solvent approach (DSA) in which the volume of added aqueous solution is slightly less than the pore volume of UiO-66 [24–26]. To simultaneously encapsulate Cu QDs into the cavities and load Cu NPs onto the surface of UiO-66, we used an advanced double-solvent approach (ADSA) in which the volume of added aqueous solution is slightly larger than the pore volume of UiO-66. By this way, most of the Cu is encapsulated in the pores while a small portion of Cu is embedded on the surface of UiO-66 in the form of NPs after reduction treatment in a H₂/Ar atmosphere.
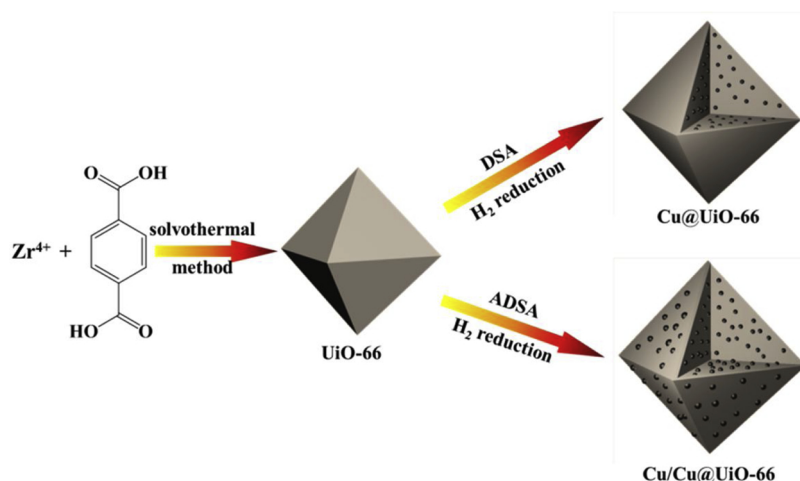

Scheme 1. Schematic for the synthesis of Cu@UiO-66 and Cu/Cu@UiO-66 via DSA and ADSA, respectively.

2. Experimental section

All the analytical grade chemicals were purchased from commercial sources and used without further treatment.

2.1. Preparation of catalysts

2.1.1. Preparation of UiO-66

UiO-66 was synthesized according to the process reported elsewhere with a slight modification [24]. Typically, $ZrCl_4$ (0.233 g, 1.0 mmol) and benzene-1,4-dicarboxylic acid (0.166 g, 1.0 mmol) were dissolved in dimethylformamide (DMF, 50 mL). Then 5 mL of acetic acid was added. The mixture was introduced into a teflon-lined autoclave of 100 mL and heated at 393 K for 40 h in an oven under static condition. Upon cooling down to room temperature, the white suspension of UiO-66 was collected by centrifugation, thoroughly washed with DMF, ethanol, and deionized water several times, and then dried under vacuum at 353 K overnight.

2.1.2. Preparation of 0.1%Cu/Cu@UiO-66 (CUO-0.1)

$0.1\%Cu^{2+}/Cu^{2+}$@UiO-66 was prepared using an advanced double solvents approach (ADSA). In a typical run, 300 mg of UiO-66 was suspended in dry n-hexane (50 mL) which is hydrophobic. The mixture was sonicated for 30 min to ensure uniform dispersion of UiO-66. Then 0.45 mL of aqueous $Cu(NO_3)_2$ (0.01 mol/L; m_{Cu}:m_{MOF} = 0.00096:1) was introduced dropwise into the flask under vigorous stirring, and the resulted mixture was stirred for another 5 h. The as-generated light-blue powder was separated and dried in air at room temperature before being further dried overnight at 353 K under vacuum. The $0.1\%Cu^{2+}/Cu^{2+}$@UiO-66 sample was heated in a stream of 5% H_2/Ar (3 mL/min) at 623 K for 2 h to yield $0.1\%Cu/Cu$@UiO-66 (denoted herein as CUO-0.1).

2.1.3. Preparation of 0.25%Cu/Cu@UiO-66 (CUO-0.25)

For comparison, 0.25%Cu/Cu@UiO-66 (CUO-0.25) was also synthesized using ADSA to evaluate the influence of the concentration of precursor solution. First, 300 mg of UiO-66 was suspended in dry n-hexane (50 mL) and subjected to 30 min of sonication. Then 0.45 mL of aqueous $Cu(NO_3)_2$ (0.025 mol/L; m_{Cu}:m_{MOF} = 0.0024:1) was added dropwise under vigorous stirring. The steps that followed were the same as those for the generation of CUO-0.1.

2.1.4. Preparation of 0.05%Cu@UiO-66 and 0.1%Cu@UiO-66

For comparison, 0.05%Cu@UiO-66 and 0.1%Cu@UiO-66 were prepared via double-solvent approach (DSA). The volume of the precursor solution is subjected to the pore volume of pristine UiO-66 which is 0.85 cm^3/g. First, 300 mg of UiO-66 was suspended in dry n-hexane (50 mL) and subjected to 30 min of sonication before dropwise addition of 0.25 mL of aqueous $Cu(NO_3)_2$ (for 0.05%Cu@UiO-66, 0.01 mol/L, m_{Cu}:m_{MOF} = 0.00053:1; for 0.1%Cu@UiO-66, 0.02 mol/L, m_{Cu}:m_{MOF} = 0.00106:1) under vigorous stirring. The steps that followed were the same as those for the generation of CUO-0.1.

2.1.5. Preparation of 0.1%Cu/UiO-66

For comparison, 0.1%Cu/UiO-66 was prepared via wet impregnation. An aqueous solution containing 0.30 mg of $Cu(NO_3)_2$ was added dropwise to 300 mg of UiO-66 (m_{Cu}:m_{MOF} = 0.00102:1) with vigorous agitation. The resulted slurry was stirred for over 30 min and then dried at room temperature. The sample was heated at 623 K for 2 h in the presence of 5% H_2/Ar to afford 0.1%Cu/UiO-66.

2.1.6. Preparation of 0.1%Ag/Ag@UiO-66 (AUO-0.1)

The steps for the synthesis of AUO-0.1 were the same as those of CUO-0.1, except that 0.45 mL of aqueous $AgNO_3$ (0.006 mol/L) was used as precursor solution.

2.2. Photocatalytic activity measurements

The photocatalytic performance of the catalysts was evaluated in the photocatalytic oxidation of benzyl alcohol under ambient conditions (i.e., room temperature and atmospheric pressure). Typically, 20 μL of alcohol and 32 mg of catalyst were mechanically mixed with 3 mL of acetonitrile in a round bottom flask. A condenser pipe was installed to trap benzyl alcohol and products. To disperse the catalyst evenly in the solution, the suspension was stirred for 30 min under a flow of O_2 (2 mL/min). The reaction was carried out by subjecting the suspension to visible-light irradiation under a 300 W Xe lamp (PLS-SXE 300C, Perfectlight) with a 400 nm cut-off filter ($\lambda \geq 400$ nm). As for UV–vis-light irradiation, the reaction was carried out with the light filter removed. After reaction, the mixture was subjected to centrifugation for complete removal of catalyst particles, and the products were analyzed using a SHIMADZU Gas Chromatograph (GC-2010, with a capillary SHRtx-1701 analysis column).

Conversion of aromatics and selectivity to the corresponding aldehydes is defined as follows:

$$Conversion(\%) = \frac{\text{moles of alcohol reacted}}{\text{moles of alcohol supplied}} \times 100\%$$

$$Selectivity(\%) = \frac{\text{moles of aldehyde formed}}{\text{moles of alcohol reacted}} \times 100\%$$

2.3. Catalyst characterizations

The Cu content of samples were calculated based on the data of elemental analysis collected by means of inductively coupled plasma atomic emission spectroscopy (ICP-AES). The morphology and microscopic structure were analyzed using a scanning electron microscope (FE-SEM, Hitachi S-4800) and a high-resolution transmission electron microscope (HR-TEM, JEM-2100 F). The crystal phase of samples was determined over a Bruker D8 Advance X-ray diffractometer with monochromatized Cu-Kα radiation (λ = 0.154 06 nm). The X-ray photoelectron spectroscopic (XPS) results (Cu 2p, Zr 3d, C 1 s and O 1 s) of surface species were collected over a VG Multilab 2000 equipment using Mg-Kα (hν = 1253.6 eV) as excitation source (XPS, SSX-100). The UV–vis diffuse reflectance spectra (UV–vis DRS) were obtained over a Cary-100 spectrophotometer, using $BaSO_4$ background as reference. Brunauer–Emmett–Teller (BET) surface areas of samples were determined by nitrogen adsorption–desorption isotherm measurements (77 K) over a Micromeritics Tristar-3000 nitrogen adsorption apparatus. Photoluminescence (PL) spectra were acquired over a Shimadzu RF-5301PC fluorescence spectrophotometer. Electron spin resonance spectra were recorded on a JES-FA200 electron paramagnetic resonance spectrometer at room temperature in the absence or presence of light irradiation.

2.4. Photo-electrochemical measurements

Photocurrent measurement was performed on a CHI660E electrochemistry workstation at room temperature. The experiments were carried out in a standard three-electrode cell that contained a Na_2SO_4 aqueous solution (0.2 mol/L), with a platinum foil and a saturated calomel electrode as counter electrode and reference electrode, respectively. To prepare the working electrodes, a slurry containing 40 mg of as-prepared photocatalyst, 10% DMF and 10% nafion was prepared and coated on pieces of FTO (fluorine-doped tin oxide), which were ultrasonically cleaned in soap-suds, deionized water, and acetone successively. Then the FTO pieces were dried in air at 333 K for 6 h. The area of the working electrodes was roughly 2 × 2 cm^2. A 500 W Xe lamp with a 400 nm cut-off filter was used as light source.

3. Results and discussion

According to the SEM images, UiO-66 octahedrons with size of ca. 500 nm (Fig. 1a) were successfully synthesized, in agreement with reported results [24,27–29]. As shown in Fig. 1b, the octahedral morphology is maintained after Cu modification and calcination. As indicated by the TEM images, there is no detection of nanoparticles on the surface of all samples except for CUO-0.25 with high Cu loading (Fig. 1c–f). In the HRTEM images (insets of Fig. 1c–f), particles with lattice fringe distance of 0.209 nm corresponding to (111) plane of Cu° can be seen, and the Cu particle size of CUO-0.1, 0.05%Cu@UiO-66 and CUO-0.25 is estimated to be ca. 1, 1 and 10 nm, respectively. The results of powder X-ray diffraction (XRD) analysis confirm that there is no apparent loss of UiO-66 crystallinity and structure upon the generation of CUO-0.1 (Fig. 2a). Over CUO-0.1, the diffraction peaks of Cu NPs are not identifiable, implying that the Cu NPs are small in size and low in content. In contrast, the higher intensity of these peaks in the cases of 0.1%Cu/UiO-66 and CUO-0.25 indicates that there are larger amount of copper on the UiO-66 surface (Fig. S1 of supporting information, SI). According to N_2 sorption isotherms (Fig. 2b), the BET surface area of UiO-66, 0.05%Cu@UiO-66, CUO-0.1 and CUO-0.25 is 1460, 1084, 1007 and 782 m^2 g^{-1}, respectively. The appreciable decrease in specific surface area indicates high dispersion of Cu NPs into the cavities of UiO-66 [13]. In addition, the results of TEM observation reveal that the size of Cu NPs is around 1 nm, which is close to the pore size of UiO-66 (Fig. S2 and S3, SI). In the HRTEM image of CUO-0.1, lattice fringe with distance of 0.209 nm corresponds to (111) planes of Cu° NPs can be

detected.

As shown in Table 1, the actual Cu and Ag contents of the metal-modified UiO-66 samples were analyzed by ICP-AES. Despite the trend of actual amounts of Cu is agreeable with the nominal values, it is apparent that the former is lower than the latter. In XPS analysis of CUO-0.1, Cu 2p signals can hardly be detected; the result evidences that the presence of Cu on the surface of CUO-0.1 is ultralow (Fig. S4, SI). The FT-IR spectra of UiO-66 and CUO-0.1 are shown in Fig. S5 (SI). The typical stretching modes of −OH located at 3600~2500 cm^{-1} are observable for both UiO-66 and CUO-0.1, along with the vibration peak at 772 and 652 cm^{-1}, which are characteristic absorption peaks of benzene units. The absorption pattern of CUO-0.1 is similar to that of UiO-66, indicating that the copper of CUO-0.1 is present in elemental form. As revealed in Fig. S6 (SI), the powder of UiO-66 and 0.05%Cu@UiO-66 are pure white, while that of CUO-0.1 and CUO-0.25 are light yellow. The difference in colour between these samples is attributed to the Cu NPs on the external surface of UiO-66.

The optical responses of CUO-0.1 and reference samples were examined by UV–Vis spectra (Fig. 3). It is confirmed that UiO-66 and Cu@UiO-66 have no absorption in the visible-light region. As for CUO-0.1, 0.1%Cu/UiO-66 and CUO-0.25, there is absorption peak at approximately 400 nm ($λ_{max}$ = 355 nm). There is no absorption band at 550–700 nm ascribable to the plasmon absorption of large Cu NPs for sizes close to 50 nm, indicating that the Cu NPs in our case are below 50 nm [30–33]. Actually, compared with those of previous report, the sizes the Cu NPs in the present case are below 3 nm [34]. Noted that the absorption peaks in the UV region belong also to plasmonic absorption, and we can attribute them to the plasmon effect of Cu [35]. The result was further confirmed by disappearance of the peak at $λ_{max}$ = 355 nm after been annealed at 673 K for 4 h in air. Even with Cu loading, there is no detection of plasmon resonance absorption peak of Cu in the cases of 0.05%Cu@UiO-66 and 0.1%Cu@UiO-66, implying successful encapsulation of Cu nanoparticles inside UiO-66 as well as the absence of Cu nanoparticles on the surface of UiO-66. Corresponding to that, the photocurrent responses of UiO-66, 0.05%Cu@UiO-66 and 0.1%Cu@UiO-66 are close to zero under visible-light irradiation (Fig. 4a). Nonetheless, all of them are excited by UV light (Fig. 4b). With Cu encapsulated in UiO-66, 0.05%Cu@UiO-66 and 0.1%Cu@UiO-66 exhibit various degrees of enhancement in photocurrent intensity. The phenomenon indicates with the encapsulation of Cu QDs in UiO-66, there is the formation of Cu-MOF Schottky junctions that enable efficient transport of photo-generated electrons from MOF. In addition, Fig. 4 reveals that with the presence of Cu NPs on the external surface of UiO-66, there is photocurrent response under visible-light irradiation. Among the synthesized samples, CUO-0.1 shows the strongest photocurrent intensity disregard the wavelength of light source. Plausibly the phenomenon is a result of synergism between Cu plasmon resonance and Cu-MOF Schottky junction. The CUO-0.25 sample shows photocurrent intensity less than that of CUO-0.1, mainly because the aggregation of Cu NPs makes the transfer of hot electrons difficult. As a result, there is increased probability of electron-hole recombination.

Photoluminescence (PL) emission spectroscopy can offer important information related to photo-induced charge transfer and recombination. The PL intensity in the UV region is almost quenched upon the incorporation of Cu QDs into UiO-66 (Fig. 5a), suggesting that the formation of Cu-MOF Schottky junctions prevents the recombination of photo-induced charge carriers. In the visible region (Fig. 5b), the PL intensity of UiO-66, 0.05%Cu@UiO-66 and 0.1%Cu@UiO-66 are close to zero because they are not responsive to visible light. It is deduced that CUO-0.1 has the highest e$^-$–h$^+$ separation efficiency among the prepared catalysts. The distinct difference in optical and electrochemical properties among the samples infers discrepancy in photocatalytic activity, and that CUO-0.1 is the best in photocatalytic performance.

We then investigated the selective oxidation of benzyl alcohol (BA) under different conditions (Table 2). Entry 1 shows that there is almost
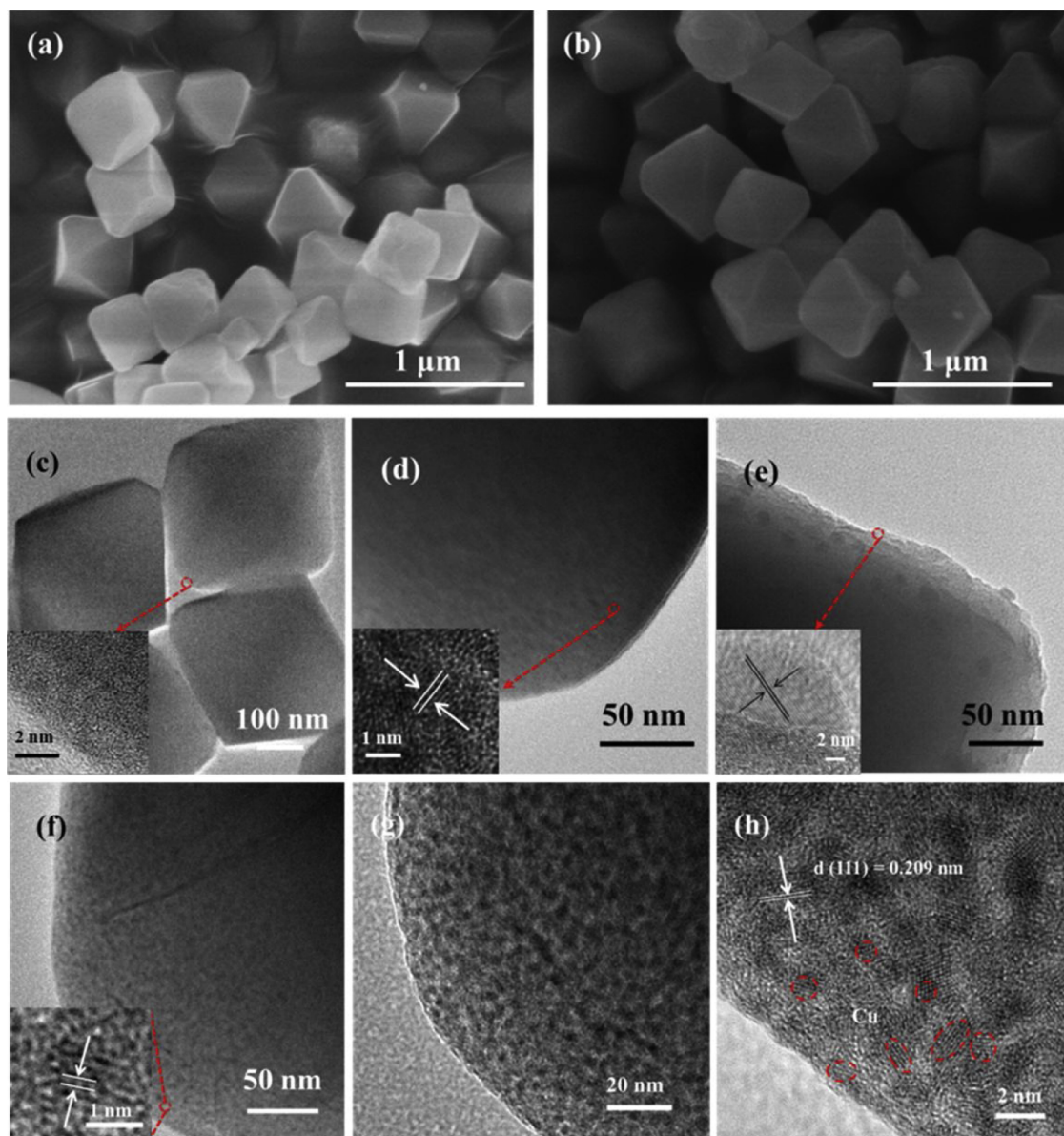
Fig. 1. (a) (b) SEM images of UiO-66 and CUO-0.1, (c) (d) (e) (f) TEM images of UiO-66, 0.05%Cu@UiO-66, CUO-0.25 and CUO-0.1, respectively, with HRTEM images shown as insets, (g) (h) high-resolution TEM (HRTEM) images of CUO-0.1 at different magnifications (the Cu entities are highlighted in red circles) (For interpretation of the references to colour in this figure legend, the reader is referred to the web version of this article).
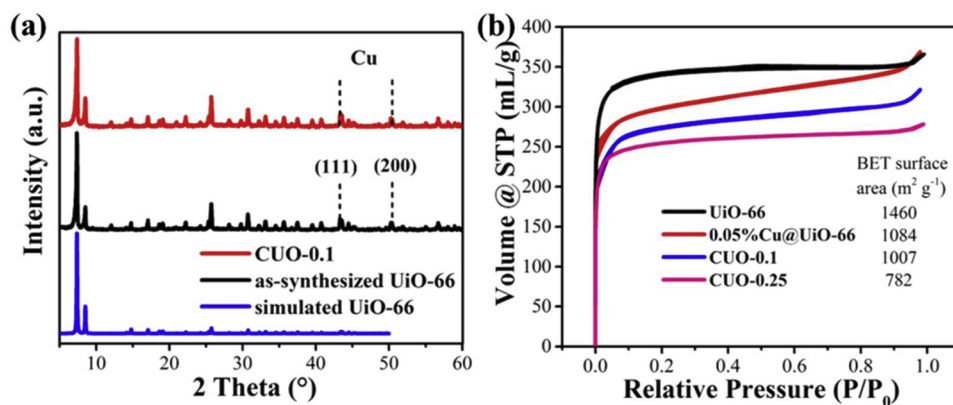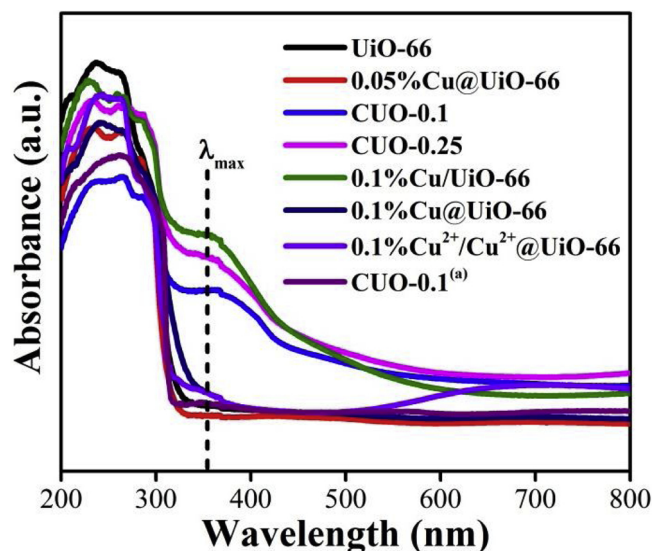

Fig. 2. (a) XRD patterns of simulated UiO-66, as-synthesized UiO-66, and CUO-0.1. (b) N_2 sorption isotherms of UiO-66 and CUO-0.1 at 77 K with the BET surface area data provided as inset.

Table 1
Copper (or silver) content of different catalysts according to ICP-AES analysis.

Samples	Cu (Ag) Content (%)
0.05%Cu@UiO-66	0.028
CUO-0.1	0.058
CUO-0.25	0.160
0.1%Cu@UiO-66	0.061
0.1%Cu/UiO-66	0.057
AUO-0.1	0.053

Fig. 3. UV–vis diffuse reflectance spectra of the prepared samples (λ_{max} = 355 nm). [a] Annealed at 673 K for 4 h in air.

no conversion of BA in the absence of catalyst. Entry 2 indicates that in the presence of CUO-0.1, BA conversion is 3.2% in the dark. The result implies CUO-0.1 can catalyze the oxidation of BA without light at ambient temperature [36]. Entry 3 shows that the conversion of BA in air is similar to that in oxygen, indicating that the reaction does not require a high level of oxygen. The test on copper powder demonstrates that large-size Cu particles loaded on UiO-66 have poor efficiency in the conversion of BA (Entry 4). Entry 5 shows that CuO is poor in BA conversion, evidencing that the photocatalytically active sites are from metallic Cu rather than CuO on UiO-66. Experiments with different solvents show that the strong oxygen uptake ability of benzotrifluoride can promote the conversion of BA, and BA conversion reaches an admirable value of 79.5% under UV–vis light irradiation. When using light with a wavelength of 400 ± 20 nm, the conversion of BA is

similar to that under visible light, indicating that the visible-light-driven activity of CUO-0.1 is mainly ascribed to Cu loaded on the surface of UiO-66. It is worth pointing out that the as-prepared CUO-0.1 photocatalyst shows much higher activity than AUO-0.1, with the latter having Ag instead of Cu loaded on UiO-66.

The selective oxidation of BA under visible light irradiation ($\lambda \geq 400$ nm) over different catalysts was also investigated. As displayed in Fig. 6a, UiO-66, 0.05%Cu@UiO-66 and 0.1%Cu@UiO-66 exhibit negligible activities. With Cu NPs on the surface of UiO-66, CUO-0.1 displays admirable photocatalytic activity, giving benzaldehyde yield of 49.5%. Due to aggregation of Cu NPs, CUO-0.25 and 0.1%Cu/UiO-66 are less effective than CUO-0.1. Note that UiO-66 cannot be excited by visible light, and the above photocatalytic activities directly reflect the effects of Cu plasmon and hot-electron migration. In addition, only benzaldehyde could be detected as product in the oxidation of BA over all of the samples. To reveal the effect of Cu-MOF Schottky junctions, we monitored the reaction under the same experimental conditions, except using ultraviolet-visible light for irradiation. As shown in Fig. 6b, 0.05%Cu@UiO-66 and 0.1%Cu@UiO-66 that have almost no Cu NPs on the external surface show better benzaldehyde yields than UiO-66. The conversion of BA over UiO-66, 0.05%Cu@UiO-66 and 0.1%Cu@UiO-66 is 30.8%, 49.4% and 53.3%, respectively. The results suggest that due to the existence of Cu-MOF Schottky junctions in 0.05%Cu@UiO-66 and 0.1%Cu@UiO-66, there is acceleration of electron migration. Moreover, owing to the synergism of SPR and Schottky junctions, CUO-0.1 has the highest photocatalytic activity among the synthesized catalysts. Among the many catalysts for partial oxidation of benzyl alcohol, CUO-0.1 is moderately high in photocatalytic activity (Table S1).

There is no apparent loss of catalytic activity across five consecutive runs over CUO-0.1 (Fig. 6b). The TEM image and XRD pattern of a used CUO-0.1 sample are shown in Fig. S7 (SI). While the Cu QDs are encapsulated in the cavities of UiO-66, the Cu NPs on the external surface display size distribution largely similar to that of fresh CUO-0.1. The appearance of nanoparticles of bigger diameter is a sign of aggregation of Cu NPs. In general, CUO-0.1 possesses considerable stability for the photocatalytic reaction.

We also studied the effect of *para*-substitution on the aromatic ring (Table 3). It is found that electron-donating substituents enhance BA conversion, whereas strong electron-donating substituents such as OCH_3 slightly reduce the selectivity to benzaldehyde. The phenomena could be due to the formation of electron-deficient intermediates that favours the photocatalytic oxidation of aromatic alcohols to aldehydes. Weak electron-withdrawing substituents, such as Cl, also increase BA conversion. However strong electron-withdrawing substituents, such as NO_2, passivate the benzene ring and reduce BA conversion.

To decode the synergism of plasmonic effect of Cu NPs and Cu-MOF Schottky junctions in the boosting of BA conversion, we performed Mott-Schottky measurements in conjunction with electron spin
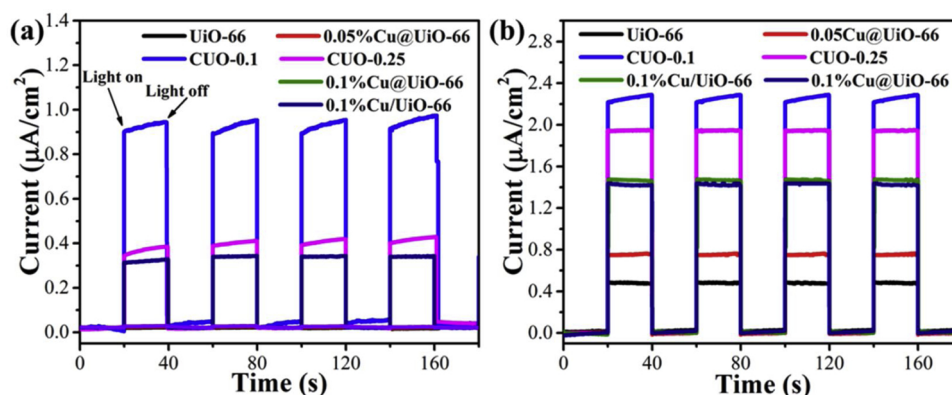
Fig. 4. Photocurrent responses under (a) visible-light ($\lambda \geq 400$ nm) and (b) ultraviolet-visible light ($\lambda = 300~800$ nm) irradiation.
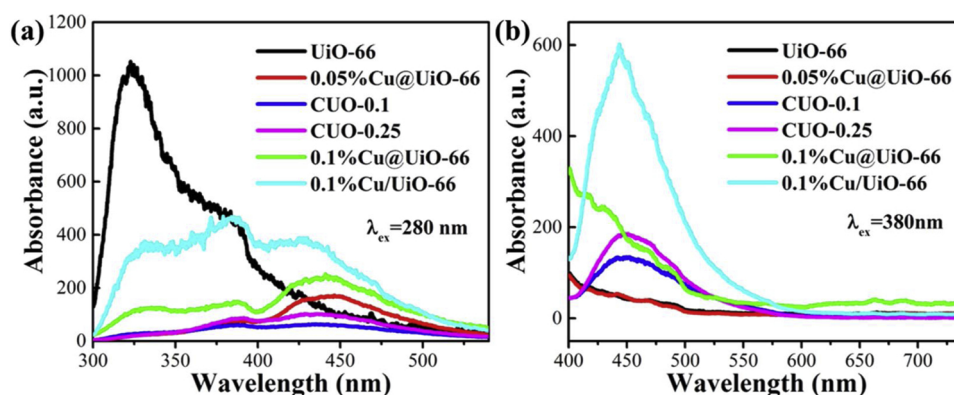
Fig. 5. (a) PL emission spectra (λ_{ex} = 280 nm); and (b) PL emission spectra (λ_{ex} = 380 nm) of prepared catalysts.

Table 2
Photocatalytic activities for selective oxidation of benzylic alcohols over CUO-0.1 and other catalysts under various conditions[a].

Entry	Catalyst	Solvent	hν	Atm.	Conv. (%)	Sel. (%)
1		Acetonitrile	+	O_2	< 0.1	
2	CUO-0.1	Acetonitrile	–	O_2	3.2	> 99
3	CUO-0.1	Acetonitrile	+	Air	46.8	> 99
4	Cu powder	Acetonitrile	+	O_2	5.3	> 99
5	0.1%CuO@UiO-66	Acetonitrile	+	O_2	3.3	> 99
6	CUO-0.1	Trifluorotoluene	+	O_2	67.5	> 99
7	CUO-0.1	Water	+	O_2	32.6	> 99
8	CUO-0.1	Toluene	+	O_2	38.9	> 99
9	CUO-0.1	Acetonitrile	+	O_2	49.5	> 99
10[b]	CUO-0.1	Acetonitrile	+	O_2	48.1	> 99
11[c]	CUO-0.1	Acetonitrile	+	O_2	79.5	92
12	AUO-0.1	Acetonitrile	+	O_2	13.6	> 99

[a] reaction conditions : substrate (0.2 mmol), catalyst (32 mg), O_2 flow rate (2 mL·min^{-1}), acetonitrile (3 mL), visible-light irradiation ($\lambda \geq$ 400 nm, 3 h); "+" and "–" indicating with or without light irradiation.
[b] λ = 400 ± 20 nm.
[c] 300 $\leq \lambda \leq$ 800 nm.

resonance (ESR) analysis. The goal is to clarify the charge transfer process of CUO-0.1. For UiO-66, there are hexameric [Zr$_6$O$_4$(OH)$_4$] which are photochromic due to the reduction of Zr^{4+} to Zr^{3+} [37,38]. To elucidate its semiconductor-like character, Mott-Schottky measurements at different frequencies were conducted (Fig. 7a). The positive slope of the obtained C^{-2} value reveals the semiconductor behavior of UiO-66 which is typically n-type, indicating migration of hot electrons from Cu NPs to the LUMO rather than the delivery of hot holes to the HOMO of UiO-66. Referring to the LUMO of UiO-66, the flat band

position is determined from the intersection, having value of -0.53 V versus Ag/AgCl (i.e., -0.33 V vs. normalized hydrogen electrode (NHE)) [4,39]. With a band gap of 3.92 eV estimated from the Tauc plot (Fig. 7b), the HOMO of UiO-66 is calculated to be 3.39 V (vs. NHE) [40], a value more positive than the redox potential of BA oxidation (+1.98 eV). More importantly, the LUMO position of UiO-66 is more negative than the O_2/O_2- potential (+0.13 V vs. NHE) [41].

Given that UiO-66 is photo-responsive only to UV light, it does not display any ESR signal both in dark and under visible-light irradiation. Upon visible-light irradiation, CUO-0.1 shows two ESR signals at g values of 2.044 and 1.988 (Fig. 8a). In order to distinguish the attribute of these two signals, we conducted control experiments over UiO-66 and CUO-0.25 (Fig. 8b). The former shows ESR signal at g value of 1.988 that can be ascribed to Zr^{3+} generated in Zr-O clusters upon UV irradiation. When CUO-0.25 is exposed to visible light, only the ESR signal at 2.044 appears, which can be attributed to plasmonic hot electrons generated by Cu NPs. When CUO-0.1 is irradiated by visible light, the plasmonic hot electrons in Cu NPs are triggered and injected into UiO-66, resulting in reduction of Zr-O clusters and the generation of Zr^{3+}. When the light is switched off, the strong Zr^{3+} signal of 0.05%Cu@UiO-66 disappears after 10 min, whereas that of UiO-66 remains, unambiguously manifesting the electron receptor role of Cu QDs in 0.05%Cu@UiO-66 (Fig. S8, SI). The results further suggest that the Cu NPs can be divided into two categories. A portion of them are incorporated uniformly into UiO-66 and the rest is loaded on the external surface of UiO-66; and all of the Cu NPs do not suffer from light-shielding effect. The consequence is direction guiding of electron migration and promotion of charge transfer, and the ability of steering electron flow ensures the outstanding photocatalytic performance of CUO-0.1.
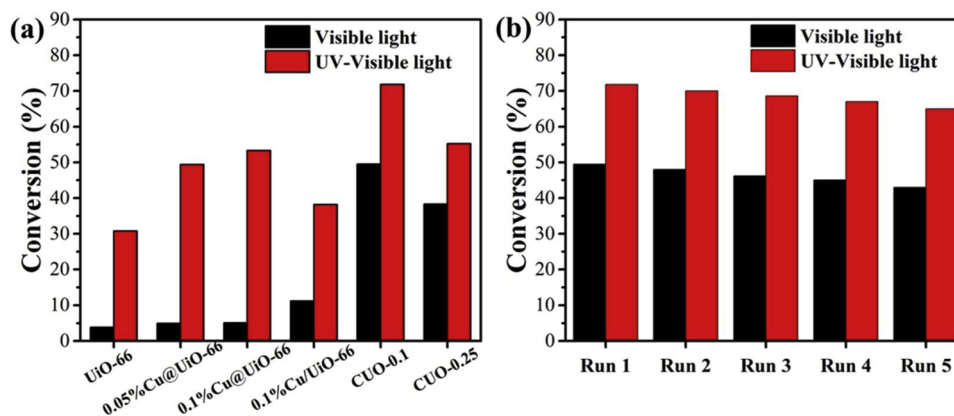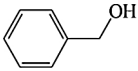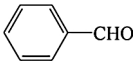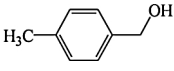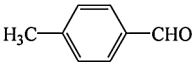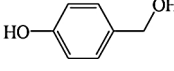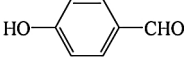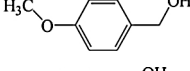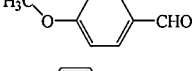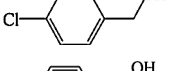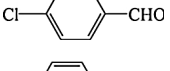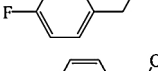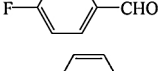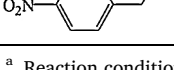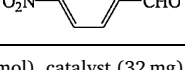

Fig. 6. (a) Conversion of BA over the synthesized catalysts under visible light or UV–vis light irradiation (from a 300 W Xe lamp) for 3 h at 298 K. Conditions: 0.2 mmol BA in 3 mL MeCN with 32 mg of photocatalyst, O_2 flow rate (2 mL·min^{-1}); (b) Recycling performance of CUO-0.1.

Table 3
Substrate scope of the photocatalytic oxidation of aromatic alcohols into aldehydes[a].

Substrate	Product	Conv. (%)	Sel. (%)	Formation Rate (µmol/g/h)
benzyl alcohol	benzaldehyde	49.5	> 99	1031
4-methylbenzyl alcohol	4-methylbenzaldehyde	50.3	> 99	1048
4-hydroxybenzyl alcohol	4-hydroxybenzaldehyde	64.6	93	1447
4-methoxybenzyl alcohol	4-methoxybenzaldehyde	69.4	90	1301
4-chlorobenzyl alcohol	4-chlorobenzaldehyde	54.5	> 99	1135
4-fluorobenzyl alcohol	4-fluorobenzaldehyde	26.6	> 99	554
4-nitrobenzyl alcohol	4-nitrobenzaldehyde	20.2	> 99	421

[a] Reaction conditions: substrate (0.2 mmol), catalyst (32 mg), O_2 flow rate (2 mL·min^{-1}), acetonitrile (3 mL), visible-light irradiation ($\lambda \geq 400$ nm, 3 h).
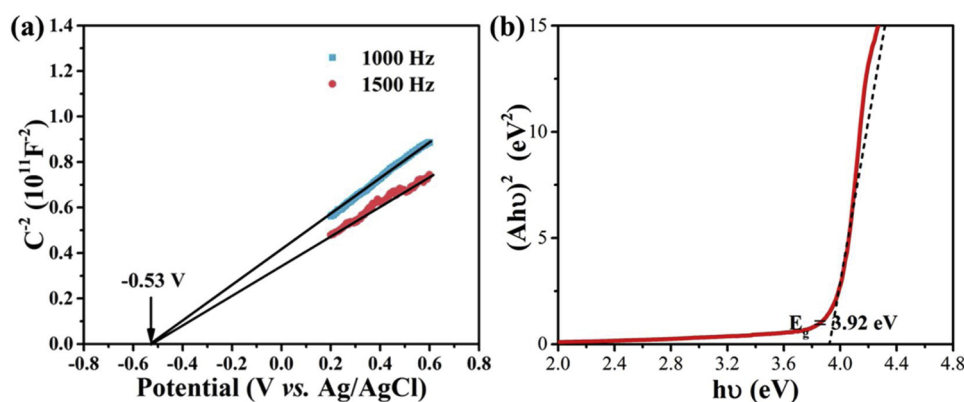
Fig. 7. (a) Mott-Schottky plot of UiO-66 in Na_2SO_4 aqueous solution (0.2 M) at frequency of 1000 and 1500 Hz. (b) Tauc plot of UiO-66 with its band gap estimated to be 3.92 eV.

Based on the fact that H_2O_2 is detected during the reaction process (Fig. S9, SI), a plausible reaction mechanism is proposed (Scheme 2). First BA and O_2 are adsorbed on UiO-66 in the dark. Under visible light illumination, the adsorbed oxygen is reduced by photo-generated electrons to superoxide radicals ($^{\cdot}O_2^{-}$), and the hot holes on the Cu NPs induce BA to release protons directly under the auxiliary of $^{\cdot}O_2^{-}$ [42,43]. As shown in Fig. S10 (SI), the detected signal reveals the superb ability of CUO-0.1 in converting O_2 to $^{\cdot}O_2^{-}$. The superoxide radicals further induce the complex to release protons, resulting in the formation of benzaldehyde and H_2O_2. Subsequently, H_2O_2 decomposes to H_2O.
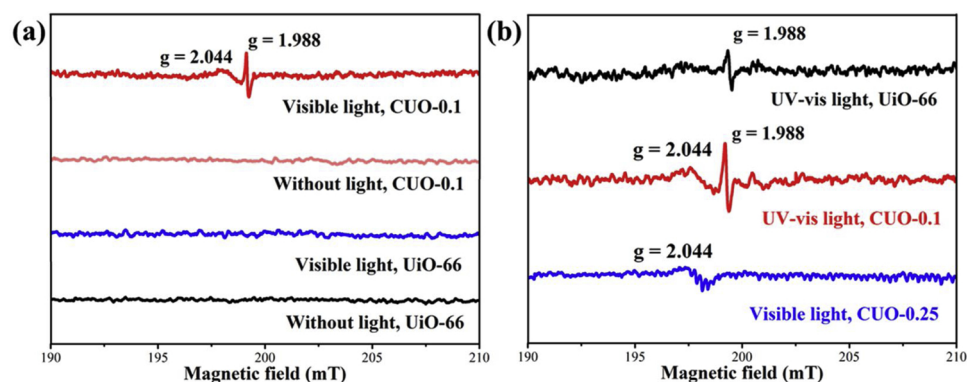
Fig. 8. UiO-66 and CUO-0.1, and (d) UiO-66, CUO-0.1 and CUO-0.25 at 298 K in the absence or presence of various light illuminations.
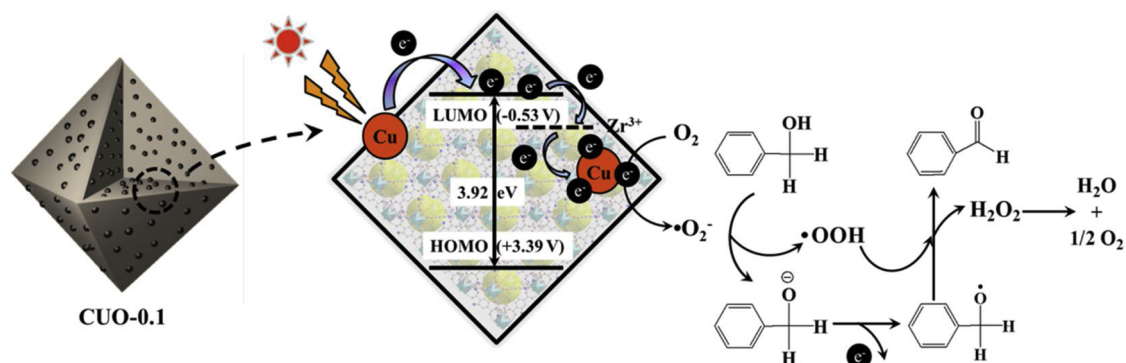
Scheme 2. Migration of electrons in CUO-0.1 according to energy levels and proposed mechanism for the selective oxidation of benzyl alcohol.

4. Conclusions

In summary, uniform Cu NPs are simultaneously incorporated into as well as supported on UiO-66, which is a MOF of wide band gap, to afford Cu/Cu@UiO-66 *via* ADSA followed by H_2 reduction. The successful synthesis of CUO-0.1 attains the synergetic deployment of visible-light-driven plasmonic hot electrons and Schottky junction for electron injection and trapping, respectively, which could greatly improve solar energy utilization and separation of photo-generated electrons and holes in UiO-66. Compared with the other Cu-loaded UiO-66 samples, CUO-0.1 exhibits enhanced photocatalytic activity under visible light irradiation, demonstrating that the composite catalyst is suitable for efficient light harvesting and charge separation. The present study demonstrates that the introduction of an ultralow amount of Cu by ADSA results in improved MOF photocatalytic activity. The present work provides a facile way for the integration of SPR effect with that of Schottky junctions for enhanced photocatalytic action.

Acknowledgements

Appendix A. Supplementary data

Supplementary material related to this article can be found, in the online version, at doi:https://doi.org/10.1016/j.apcatb.2019.02.012.

References

[1] H. Wang, X.Z. Yuan, Y. Wu, G.M. Zeng, H.R. Dong, X.H. Chen, L.J. Leng, Z.B. Wu, L.J. Peng, Appl. Catal. B: Environ. 186 (2016) 19–29.
[2] M. Wen, K. Mori, Y. Kuwahara, H. Yamashita, ACS Energy Lett. 2 (2017) 1–7.
[3] Y.Z. Chen, Z.U. Wang, H. Wang, J. Lu, S.H. Yu, H.L. Jiang, J. Am. Chem. Soc. 139 (2017) 2035–2044.
[4] J.D. Xiao, L. Han, J. Luo, S.H. Yu, H.L. Jiang, Angew. Chem. Int. Ed. 57 (2018) 1103–1107.
[5] M. Wen, Y. Kuwahara, K. Mori, H. Yamashita, Top. Catal. 59 (2016) 1765–1771.
[6] Z.Y. Jiang, X.H. Zhang, Z.M. Yuan, J.C. Chen, B.B. Huang, D.D. Dionysiou, G.H. Yang, Chem. Eng. J. 348 (2018) 592–598.
[7] W.J. He, Y.J. Sun, G.M. Jiang, H.W. Huang, X.M. Zhang, F. Dong, Appl. Catal. B: Environ. 232 (2018) 340–347.
[8] Y.J. Ma, X.Z. Zhu, S.S. Xu, G.L. He, L. Yao, N.T. Hu, Y.J. Su, J. Feng, Y.F. Zhang, Z. Yang, Appl. Catal. B: Environ. 234 (2018) 26–36.
[9] C. Wang, K.E. deKrafft, W. Lin, J. Am. Chem. Soc. 134 (2012) 7211–7214.
[10] L. Chen, H. Chen, R. Luque, Y. Li, Chem. Sci. 5 (2014) 3708–3714.
[11] Z. Guo, C. Xiao, R.V. Maligal Ganesh, L. Zhou, T.W. Goh, X. Li, D. Tesfagaber, A. Thiel, W. Huang, ACS Catal. 4 (2014) 1340–1348.
[12] Q.L. Zhu, Q. Xu, Chem. Soc. Rev. 43 (2014) 5468–5512.
[13] Y.H. Zhou, Q. Yang, Y.Z. Chen, H.L. Jiang, Chem. Commun. (Camb.) 53 (2017) 12361–12364.
[14] J. Dong, J. Ye, D. Ariyanti, Y. Wang, S. Wei, W. Gao, Chemosphere 204 (2018) 193–201.
[15] Y.B. Lou, Y.K. Zhang, L. Cheng, J.X. Chen, Y.X. Zhao, ChemSusChem 11 (2018) 1505–1511.
[16] P. Zhang, T. Song, T. Wang, H. Zeng, Appl. Catal. B: Environ. 225 (2018) 172–179.
[17] J.M. Hoover, B.L. Ryland, S.S. Stahl, J. Am. Chem. Soc. 135 (2013) 2357–2367.
[18] B.L. Ryland, S.S. Stahl, Angew. Chem. Int. Ed. 53 (2014) 8824–8838.
[19] A. Taher, D.W. Kim, I.M. Lee, RSC Adv. 7 (2017) 17806–17812.
[20] Y.Z. Chen, Q. Xu, S.H. Yu, H.L. Jiang, Small 11 (2015) 71–76.
[21] Q. Yang, Y.Z. Chen, Z.U. Wang, Q. Xu, H.L. Jiang, Chem. Commun. 51 (2015) 10419–10422.
[22] J.D. Xiao, Q. Shang, Y. Xiong, Q. Zhang, Y. Luo, S.H. Yu, H.L. Jiang, Angew. Chem. Int. Ed. 55 (2016) 9389–9393.
[23] Q. Yang, Q. Xu, S.H. Yu, H.L. Jiang, Angew. Chem. Int. Ed. 55 (2016) 3685–3689.
[24] J.H. Cavka, S. Jakobsen, U. Olsbye, N. Guillou, C. Lamberti, S. Bordiga, K.P. Lillerud, J. Am. Chem. Soc. 130 (2008) 13850–13851.
[25] C.G. Silva, I. Luz, F.X. Llabrés i Xamena, A. Corma, H. Garcia, Chem. Eur. J. 16 (2010) 11133–11138.
[26] C. Wang, Z. Xie, K.E. deKrafft, W. Lin, J. Am. Chem. Soc. 133 (2011) 13445–13454.
[27] F. Vermoortele, B. Bueken, G. Le Bars, B. Van de Voorde, M. Vandichel, K. Houthoofd, A. Vimont, M. Daturi, M. Waroquier, V. Van Speybroeck, C. Kirschhock, D.E. De Vos, J. Am. Chem. Soc. 135 (2013) 11465–11468.
[28] G.C. Shearer, S. Chavan, J. Ethiraj, J.G. Vitillo, S. Svelle, U. Olsbye, C. Lamberti, S. Bordiga, K.P. Lillerud, Chem. Mater. 26 (2014) 4068–4071.
[29] Y. Han, M. Liu, K. Li, Y. Zuo, Y. Wei, S. Xu, G. Zhang, C. Song, Z. Zhang, X. Guo, CrystEngComm 17 (2015) 6434–6440.
[30] C. Vázquez-Vázquez, M. Bañobre-López, A. Mitra, M.A. López-Quintela, J. Rivas, Langmuir 25 (2009) 8208–8216.
[31] P. Christian, M. Bromfield, J. Mater. Chem. 20 (2010) 1135–1139.
[32] W.T. Wei, Y.Z. Lu, W. Chen, S.W. Chen, J. Am. Chem. Soc. 133 (2011) 2060–2063.
[33] N. Vilar-Vidal, J. Rivas, M.A. Lopez-Quintela, ACS Catal. 2 (2012) 1693–1697.
[34] J. Feng, Y.Y. Ju, J.J. Liu, H.G. Zhang, X.G. Chen, Anal. Chim. Acta 854 (2015) 153–160.
[35] P.H. Tseng, Y.Z. Wang, T.H. Hsieh, K.S. Ho, C.H. Tsai, K.T. Chen, Nanotechnology 29 (2018) 085603.
[36] L. Shen, S. Liang, W. Wu, R. Liang, L. Wu, Dalton Trans. 42 (2013) 13649–13657.
[37] D. Sun, Y. Fu, W. Liu, L. Ye, D. Wang, L. Yang, X. Fu, Z. Li, Chem. Eur. J. 19 (2013) 14279–14285.
[38] H.Q. Xu, J. Hu, D. Wang, Z. Li, Q. Zhang, Y. Luo, S.H. Yu, H.L. Jiang, J. Am. Chem. Soc. 137 (2015) 13440–13443.
[39] J. He, J. Wang, Y. Chen, J. Zhang, D. Duan, Y. Wang, Z. Yan, Chem. Commun. 50 (2014) 7063–7066.
[40] L.N. Song, L. Chen, J. He, P. Chen, H.K. Zeng, C.T. Au, S.F. Yin, Chem. Commun. 53 (2017) 6480–6483.
[41] T. Yan, Q. Yan, X. Wang, H. Liu, M. Li, S. Lu, W. Xu, M. Sun, Dalton Trans. 44 (2015) 1601–1611.
[42] F. Su, S.C. Mathew, G. Lipner, X. Fu, M. Antonietti, S. Blechert, X. Wang, J. Am. Chem. Soc. 132 (2010) 16299–16301.
[43] K. Jing, J. Xiong, N. Qin, Y. Song, L. Li, Y. Yu, S. Liang, L. Wu, Chem. Commun. 53 (2017) 8604–8607.